CHAPTER 4 RESULT AND DISCUSSIONS

4.1 Thermodynamics Properties of Generic Law Potential

Based on the grand potential formalism introduced through Eq. (2.6), the thermodynamic properties of an ideal Bose gas can now be analyzed within the grand canonical ensemble. In this framework, the system is allowed to exchange both energy and particles with a thermal reservoir, and the particle number is controlled by the chemical potential μ. This ensemble is particularly appropriate for describing Bose–Einstein condensation, since the transition is characterized by the accumulation of a macroscopic number of particles in the ground state as the chemical potential approaches the lowest energy level.

Within the grand canonical ensemble, all thermodynamic quantities can be consistently derived from the grand potential Ω. In particular, the entropy S, particle number N, and internal energy U are obtained from the fundamental thermodynamic relations

$$\mathrm{S} = -\left(\frac{\partial \Omega}{\partial \mathrm{T}}\right)_{\mu} \tag{4.1}$$

$$\mathrm{N} = -\left(\frac{\partial \Omega}{\partial \mu}\right)_{\mathrm{T}} \tag{4.2}$$

and

$$U = \Omega - T\left(\frac{\partial \Omega}{\partial T}\right)_{\mu} - \mu\left(\frac{\partial \Omega}{\partial \mu}\right)_{T} \tag{4.3}$$

These relations form the basis for evaluating the thermodynamic behavior of the system in both the normal and condensed phases.

The onset of Bose–Einstein condensation in an ideal homogeneous Bose gas is determined by the saturation of the excited-state population. The corresponding critical temperature is given by

UNIVERSITAS ANDALAS
UNTUK KEDJAJAAN BANGSA

$$T_c = \frac{2\hbar^2\pi}{mk_B}\left(\frac{1}{\zeta(3/2)}\frac{N}{V}\right)^{\frac{2}{3}} \tag{4.4}$$

Where $\hbar$ is the reduced Planck constant, m denotes the particle mass, k_B is the Boltzmann constant, N/V is the particle number density, and $\zeta(3/2) \approx 2.612$ is the Riemann zeta function. As a representative realization, we consider rubidium-87 atoms with a number density $N/V = 1.5 \times 10^{19}\,\mathrm{m}^{-3}$ and atomic mass $m = 1.419 \times 10^{-25}\,\mathrm{kg}$, the critical temperature is $T_c = 130\,\mathrm{nK}$ (Aveline et al., 2020) . Below this temperature, the system enters the Bose–Einstein condensed phase, in which the majority of particles occupy the ground state (Pathria and Beale, 2011).

In the regime $T \leq Tc$, the thermodynamic properties of the system are governed by the thermally excited particles, while the condensed fraction does not contribute directly to entropy or internal energy. The number of excited particles is given by

$$N_T = V\left(\frac{mk_BT}{2\pi\hbar^2}\right)^{3/2} g_{3/2}(z) \tag{4.5}$$

Where V is the system volume, $z = e^{\beta\mu}$ is the fugacity, and $g_{3/2}(z)$ denotes the Bose function of order $3/2$. As the temperature decreases toward and below T_c, the fugacity approaches unity ($z \to 1$), leading to a finite number of thermally excited particles, while the remaining particles accumulate in the ground state. Bose–Einstein condensation is therefore characterized by the relation $N_0 = N - N_T$, where N_0 denotes the number of condensed particles.

Using Eq. (4.1), the entropy of the system in the condensed phase $z = 1$ becomes

$$S(T,V) = \frac{5}{2}k_BV\left(\frac{mk_BT}{2\hbar^2\pi}\right)^{\frac{3}{2}} g_{5/2}(1) \tag{4.6}$$

This result reflects a significant reduction of entropy compared to the normal phase, indicating the high degree of quantum order associated with Bose–Einstein condensation.

Finally, substituting Eqs. (4.1)–(4.2) into the definition of the internal energy yields

$$U(T,V) = \frac{3}{2} k_B T V \left(\frac{m k_B T}{2\pi\hbar^2}\right)^{3/2} g_{5/2}(1) \tag{4.7}$$

The nonlinear temperature dependence of the internal energy highlights the fundamental distinction between the thermal response of a Bose–Einstein condensed system and that of a classical ideal gas.

4.2 Quantum Otto Refrigerator

In Chapter 2, the model of a quantum Otto refrigerator was introduced within the framework of quasistatic and endoreversible thermodynamics. In this section, the formulation is further developed to obtain explicit expressions for the thermodynamic quantities used in the analysis of the results. The model combines two main assumptions: the quasistatic approach for the isentropic strokes and the endoreversible approach for the heat-exchange processes with the reservoirs.

The working medium considered is a non-interacting bosonic gas in the condensed phase confined in a three-dimensional potential. The internal energy of the system is given by the expression obtained in Eq. (4.7), where $g_{5/2}(1)$ denotes the Bose function in the condensation limit. This expression is used to determine the work and heat at each stage of the quantum Otto cycle. The quantum Otto refrigerator cycle consists of four stages: isentropic compression, isochoric heating, isentropic expansion, and isochoric cooling. The formulation of each stage is described as follows.

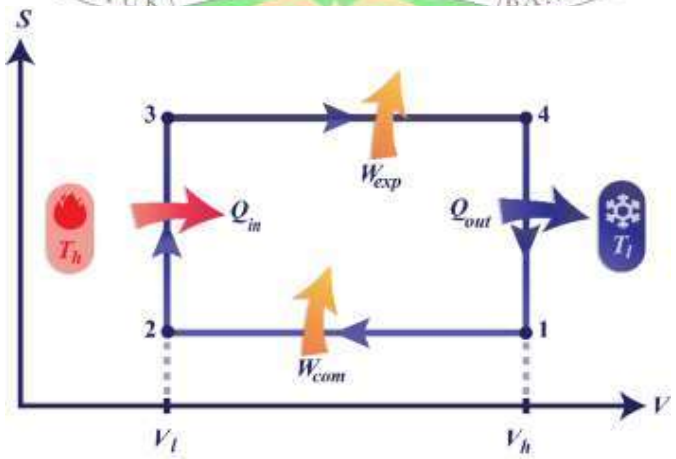

Figure 4. 1 Schematic diagram of a Quantum Otto refrigeration cycle in a three-dimensional cubic potential trap (S–V representation).

4.2.1 Isentropic Compression

Referring to the quasistatic–endoreversible model presented in Chapter 2, particularly in Eqs. (2.19) and (2.24), the work required during the isentropic compression process is obtained from the difference in the internal energy of the working medium between the initial and final states of the compression. By substituting the expression for the internal energy derived in Eq. (4.7), the compression work can be written as follows,

$$W_{comp} = \frac{3}{2} k_B \left(\frac{mk_B}{2\pi\hbar^2}\right)^{\frac{3}{2}} \left(T_2^{\frac{5}{2}} V_l - T_1^{\frac{5}{2}} V_h\right) g_{\frac{5}{2}} \tag{4.8}$$

Since the compression proceeds without heat exchange, the entropy of the system remains constant throughout the process. By applying Eq. (4.6), the corresponding relation between temperature and volume can be obtained as

$$V_h T_1^{\frac{3}{2}} = V_l T_2^{\frac{3}{2}} \tag{4.9}$$

$$T_2 = T_1 \left(\frac{V_h}{V_l}\right)^{\frac{2}{3}} \tag{4.10}$$

For convenience in the subsequent analysis, the compression ratio is defined as

$$\kappa = V_h / V_l \tag{4.11}$$

Substituting this relation into Eq. (4.1) and using the isentropic temperature relation, the compression work can be expressed as

$$W_{\text{comp}} = \frac{3}{2} k_B \left(\frac{mk_B}{2\pi\hbar^2}\right)^{3/2} T_1^{5/2} V_l \left(\kappa^{5/3} - \kappa\right) g_{5/2}(1). \tag{4.12}$$

4.2.2 Isovolume Heating

During the isochoric heating stage, the volume is kept constant at V_l, and therefore no mechanical work is performed. Referring to Eq. (2.25), the heat absorbed from the hot reservoir is determined by the change in internal energy of the working medium. By substituting the explicit form of the internal energy obtained in Eq. (4.6), the absorbed heat can be expressed as

$$Q_h = \frac{3}{2} k_B V_l \left(\frac{mk_B}{2\pi\hbar^2}\right)^{\frac{3}{2}} (T_3 - T_2)^{\frac{5}{2}} g_{\frac{5}{2}}(1) \tag{4.13}$$

The thermalization with the hot reservoir occurs over a finite time and follows the temperature evolution. Solving this relation for a heating duration τ_h gives

$$T_2 - T_h = (T_3 - T_h) e^{-\alpha_h \tau_h} \tag{4.14}$$

4.2.3 Isentropic Expansion

Referring to the quasistatic–endoreversible formulation introduced in Chapter 2, the work performed during the isentropic expansion is determined by the change in the internal energy of the working medium between states 3 and 4. By substituting the internal energy expression obtained in Eq. (4.6), the expansion work can be written as

$$W_{exp} \frac{3}{2} k_B \left(\frac{mk_B}{2\pi\hbar^2}\right)^{\frac{3}{2}} = \left(T_4^{\frac{5}{2}} V_h - T_3^{\frac{5}{2}} V_l\right) g_{\frac{5}{2}}(1) \tag{4.15}$$

Since the expansion proceeds without heat exchange, the entropy remains constant throughout the process. Using the isentropic relation introduced previously, the temperature–volume relation between states 3 and 4 can be obtained, which yields

$$T_3 = T_4 \kappa^{2/3}. \tag{4.16}$$

substituting this relation into the expression above, the expansion work can be rewritten as

$$W_{exp} = \frac{3}{2} k_B \left(\frac{mk_B}{2\pi\hbar^2}\right)^{\frac{3}{2}} T_4^{\frac{5}{2}} V_l \left(k - k^{\frac{5}{3}}\right) g_{\frac{5}{2}}(1) \tag{4.17}$$

4.2.4 Isovolume Cooling

At constant volume V_h, the heat released to the cold reservoir follows from the change in internal energy. Substituting the internal energy expression obtained in Eq. (4.6) yields

$$Q_l = \frac{3}{2} k_B \left(\frac{mk_B}{2\pi\hbar^2}\right)^{3/2} V_h \left(T_4^{5/2} - T_1^{5/2}\right) g_{5/2}(1). \tag{4.18}$$

The finite-time cooling process obeys Fourier's law, yielding the temperature evolution

$$T_1 - T_l = (T_4 - T_l)e^{-\alpha_l \tau_l}. \tag{4.19}$$

4.2 Coefficient of Performance (COP) under Partial Thermalization

Based on the calculation results obtained from Eq. (4.20), the relationship between the Coefficient of Performance (COP) and the trap geometry (volume ratio) κ is presented in Fig. 4.2. The figure shows that the COP decreases significantly as κ increases. This decreasing trend is monotonic, with the COP attaining its maximum value at small κ and continuously declining as κ is increased. For larger values of κ, the reduction in the COP becomes more pronounced, indicating that variations in κ exert a strong influence on the cooling performance of the system.

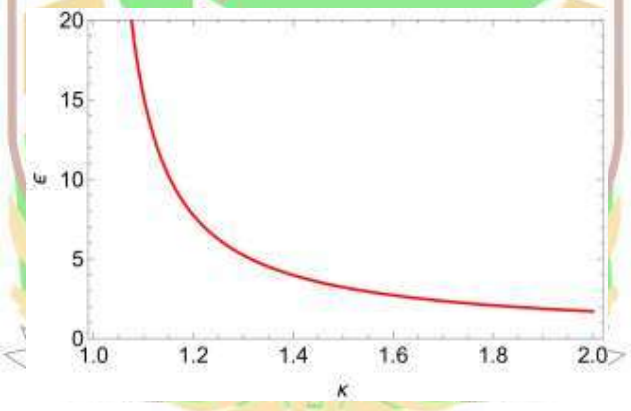

Figure 4. 2 The coefficient of performance $\boldsymbol{\varepsilon}$ as a function of the volume ratio $\boldsymbol{\kappa = V_h/V_l}$

Theoretically, the COP of a refrigeration system is defined as the ratio of the heat absorbed from the cold reservoir to the total work input supplied to the system. Under ideal and reversible conditions, the maximum attainable COP is bounded by the Carnot limit, which depends solely on the temperatures of the hot and cold reservoirs.

In the quantum Otto cycle considered in this study, the coefficient of performance (COP) is determined by the heat released to the hot reservoir, Q_h (Eq. 4.13), and the heat absorbed from the cold reservoir, Q_l (Eq. 4.18). Using the previously derived expressions for Q_h and Q_l , the COP of the quantum Otto refrigerator can be written as follows:

$$\varepsilon = \frac{1}{k^{2/3} - 1}. \tag{4.20}$$

This result shows that, in the Carnot limit, the COP depends only on the temperatures of the hot and cold reservoirs. However, within the Otto cycle, both in classical and quantum descriptions, the COP is not solely determined by the reservoir temperatures but is also influenced by internal system parameters, such as the frequency ratio or the trap volume ratio (κ) This dependence originates from the isentropic processes of the Otto cycle, during which changes in κ modify the energy-level structure of the working medium and, consequently, affect the balance between absorbed heat and input work..

In the quantum Otto model examined in this study, an increase in the κ leads to a larger modification of the energy spectrum during the isentropic processes. This enhanced spectral deformation has a direct impact on the net work required to complete one Otto cycle, resulting in a higher work input as κ increases. In contrast, the amount of heat absorbed from the cold reservoir during the isovolume processes does not increase proportionally with the work input. Consequently, the ratio between the absorbed heat and the supplied work decreases, which is manifested as a reduction in the COP, as shown in Fig. 4.2.

Beyond the effect of energy-spectrum modification, the decrease in COP is also closely associated with partial thermalization during the isovolume strokes. In this model, the contact time between the working medium and the thermal reservoirs is finite, preventing the system from reaching full thermal equilibrium. As a result, the thermal state of the working medium after the isovolume processes deviates from the ideal equilibrium state, leading to a smaller amount of exchanged heat compared to the quasistatic limit.

The combined effect of the increased work input due to a larger κ and the reduced heat absorption caused by partial thermalization is responsible for the pronounced decrease in the COP. This behavior is further amplified by the growing irreversibility of the system. Partial thermalization inherently indicates nonequilibrium dynamics accompanied by entropy production. Such entropy production represents a loss of useful work that could otherwise contribute to the cooling process, thereby degrading the overall thermodynamic performance of the refrigerator.

The behavior observed in the COP as a κ curve indicates that the system progressively departs from the quasistatic regime. In this non-quasistatic regime, increasing the speed of the cycle or enlarging internal parameter variations generally leads to a deterioration of performance. This reflects a fundamental trade-off between cooling performance and operational characteristics, where enlarging internal parameter changes does not necessarily result in an improved refrigeration efficiency.

Overall, the results demonstrate that increasing κ significantly enhances the work input required per cycle in the quantum Otto refrigerator, while the heat absorbed from the cold reservoir fails to increase accordingly. As a consequence, the COP decreases with increasing κ. This behavior highlights the non-ideal nature of the quantum Otto cycle under large internal parameter variations and limited thermal relaxation. Similar qualitative features are widely discussed in the quantum thermodynamics literature, particularly in studies of quantum Otto machines operating far from the quasistatic limit, where system performance is strongly influenced by internal parameter changes and nonequilibrium effects.

4.2 Power

Figure 4.3 illustrates the characteristics of the dimensionless power output ($P*$) as a function of the Coefficient of Performance (COP) for a quantum Otto refrigerator operating under four different thermalization regimes. The numerical results indicate that the power performance is not solely governed by the total cycle

duration, but is strongly dictated by how the available time is allocated between the isovolume heating and cooling stages. In the slow symmetric configuration (bluecurve, $\tau_h = \tau_l = 10$). The system yields the lowest power output due to the excessively long cycle time. Although this regime approaches quasistatic operation and thus favors reversibility, the extended cycle duration suppresses the achievable power.

When the cycle duration is symmetrically reduced (red curve, $\tau_h = \tau_l = 5$), the power output increases significantly. This behavior demonstrates that shortening the cycle time enhances the power output, albeit at the expense of imperfect thermalization and increased irreversibility. However, the maximum power is not obtained in this symmetric fast regime. Instead, the optimal performance emerges in the asymmetric configuration represented by the orange curve ($\tau_h = 2.5, \tau_l = 7.5$). This observation indicates that the temporal distribution between the isovolume heating and cooling processes plays a more decisive role in determining performance than the total cycle duration itself.

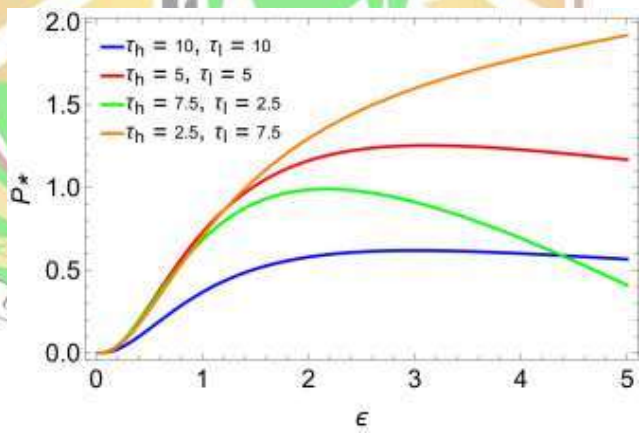

Figure 4. 3 The dimensionless power output ($\boldsymbol{P}^*$) versus the COP ($\boldsymbol{\varepsilon}$) for a quantum Otto refrigerator with various time stroke.

This behavior is rooted in the principles of quantum thermodynamics, where system performance is determined not only by thermodynamic quantities but also by the duration of each process within a cycle. The power output is defined as the net work produced during the isentropic strokes, normalized by the total cycle time (Myers et al., 2022b). In the present model, the total cycle duration is primarily

governed by the two isovolume processes, namely heating and cooling, which occur over finite time intervals τ_h and τ_l respectively. Accordingly, the expression for the power output is given in Eq (3.2). For convenience, the prefactor appearing in the internal energy of the bosonic working medium is defined as

$$A = \frac{3}{2} k_B \left(\frac{m k_B}{2\pi\hbar^2}\right)^{\frac{3}{2}} g_{\frac{5}{2}}(1). \tag{4.21}$$

Using this definition, the power output can be written in dimensionless form as

$$P^* = \frac{P}{A} \tag{4.22}$$

By combining the isentropic compression and expansion works and substituting the temperature–volume relation for the isentropic strokes, the dimensionless power output can be expressed in a compact form as

$$P^* = \frac{V_l \left(k^{\frac{2}{3}} - 1\right)\left(T_1^{\frac{5}{2}} - T_4^{\frac{5}{2}}\right)}{\gamma(\tau_h + \tau_l)} \tag{4.23}$$

Equation (4.23) clearly shows that the power output is governed by three main factors: the compression ratio κ, the temperature difference between the two adiabatic junction points T_1 and T_4, and the total cycle time dominated by the finite-duration isochoric processes.

Within this framework, the system temperatures at the transition points between isentropic and isovolume processes, namely T_1 and T_4, are not directly assumed to be identical to the reservoir temperatures. Instead, temperature evolution follows a modified version of Fourier's law adapted for finite-time interactions (Bagnato et al., 1987; Myers et al., 2022b; Zettira et al., 2024). Based on the exponential solution of linear differential equations, the following expressions are obtained

$$\mathrm{T_1} = \frac{\kappa^{2/3}(e^{\alpha_l \tau_l} - 1)\mathrm{T_l} + (1 - e^{-\alpha_h \tau_h})\mathrm{T_h}}{\kappa^{2/3}(e^{\alpha_l \tau_l} - e^{-\alpha_h \tau_h})}, \tag{4.24}$$

$$T_4 = \frac{(e^{\alpha_h \tau_h} - 1)T_h + \kappa^{2/3}(1 - e^{-\alpha_l \tau_l})T_l}{\kappa^{2/3}(e^{\alpha_h \tau_h} - e^{-\alpha_l \tau_l})}, \tag{4.25}$$

α_l, α_h are the heat transfer coefficients during isovolume interaction with the cold and hot reservoirs, respectively. By substituting T_1 and T_4 into the internal energy expressions, and combining them in the isentropic work terms, the output power per cycle can be expressed as

$$P = \frac{\frac{3}{2} k_B V_l \left(\frac{m k_B}{2\pi\hbar^2}\right)^{3/2} \zeta\left(\frac{5}{2}\right)}{\gamma(\tau_h + \tau_L)(1+\varepsilon)^{5/2}(e^{\alpha_l \tau_l + \alpha_h \tau_h} - 1)^{5/2}} \times \left\{ \left[T_l \left(\frac{1}{\varepsilon} + 1\right) e^{\alpha_h \tau_h}(e^{\alpha_l \tau_l} - 1) + T_h(e^{\alpha_h \tau_h} - 1) \right]^{5/2} - \left[T_h e^{\alpha_l \tau_l}(e^{\alpha_h \tau_h} - 1) + T_l \left(\frac{1}{\varepsilon} + 1\right)(e^{\alpha_l \tau_l} - 1) \right]^{5/2} \right\} \tag{4.26}$$

From a physical perspective, the superior performance of the asymmetric orange configuration originates from more effective entropy management and heat exchange. By allocating a longer duration to the isovolume cooling stage ($\tau_l = 7.5$), the bosonic working medium is provided with sufficient time to maximize heat extraction from the cold reservoir. Conversely, shortening the isovolume heating stage ($\tau_h = 2.5$) limits the interaction with the highly entropic hot reservoir, thereby suppressing dissipative losses and internal entropy production. This strategic asymmetry ensures that the energetic gain from heat extraction significantly outweighs the "time cost" of the cycle, while the isentropic strokes are assumed to remain adiabatic and entropy-free.

A direct comparison with the opposite asymmetric configuration (green curve, $\tau_h = 7.5, \tau_l = 2.5$) further reinforces this interpretation. Although both configurations share the same total cycle duration ($\tau = 10$), the power output of the green curve is markedly lower. In this case, the prolonged isovolume heating stage becomes counterproductive, as it enhances irreversibility without improving cooling capacity. The insufficient cooling duration prevents efficient heat

absorption from the cold reservoir, while the extended interaction with the hot reservoir leads to increased energy dissipation due to entropy.

Overall, these results confirm the existence of a fundamental trade-off between power output and irreversibility in quantum Otto refrigerators. Operation near the quasistatic limit yields low power due to long cycle durations, whereas higher power is achieved by departing from thermal equilibrium through partial thermalization. Notably, the maximum power in this study is not attained under symmetric timing conditions, but rather through an asymmetric allocation of thermalization times. This finding highlights cycle-time control as a key optimization parameter in realistic quantum Otto refrigeration systems, beyond conventional control of reservoir temperatures or trapping volumes.

4.3 Cooling Rate

The cooling rate (R) is a key performance indicator of a quantum Otto refrigerator, as it directly quantifies the system's ability to extract heat from the cold reservoir per unit time. Unlike the coefficient of performance, which emphasizes efficiency, the cooling rate provides a more practical measure of refrigeration performance under realistic operating conditions, particularly in the finite-time regime (Abah et al., 2020; Long and Liu, 2015).

$$\mathrm{R} = \frac{\mathrm{Q_l}}{\tau} = \frac{\mathrm{Q_l}}{\gamma(\tau_\mathrm{h} + \tau_\mathrm{l})}, \tag{4.27}$$

where γ is a time-scaling factor, and τ_h , τ_l denote the thermalization times during isovolume interaction with the hot and cold reservoirs, respectively. In this model, the heat absorbed from the cold reservoir is derived from the change in internal energy during the isovolume cooling process at low volume (V_l). The internal energy of working medium scales with temperature as $U \propto T^{5/2}$. Accordingly, the cooling power can be expressed as:

$$\mathrm{R} = \frac{\frac{3}{2}\mathrm{k_B}\left(\frac{\mathrm{mk_B}}{2\pi\hbar^2}\right)^{3/2} \mathrm{g}_{5/2}(1)\mathrm{V_h}(\mathrm{T_4} - \mathrm{T_1})^{5/2}}{\gamma(\tau_\mathrm{h} + \tau_\mathrm{l})}, \tag{4.28}$$

with T_1andT_4 obtained from partial thermalization based on exponential Fourier dynamics (Sutantyo et al., 2024). Figure (4.4) illustrates the cooling rate (R) as a function of the coefficient of performance (ε) for several thermalization-time configurations. For all cases considered, the cooling rate decreases monotonically as ε increases. This behavior reveals a fundamental trade-off between cooling power and efficiency in finite-time quantum refrigeration. Operating the system at higher efficiency inevitably reduces the thermodynamic driving force for heat extraction, thereby limiting the amount of heat that can be removed from the cold reservoir per cycle.

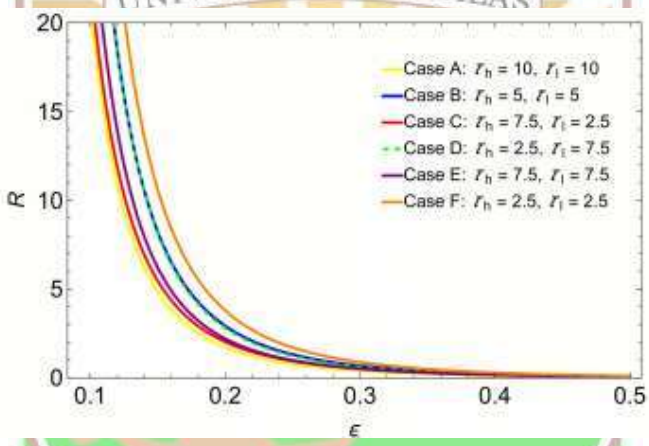

Figure 4. 4 The cooling rate $(\boldsymbol{R})$ as a function of the COP $(\boldsymbol{\varepsilon})$ with various heating and cooling stroke time.

Symmetric configurations with long thermal contact times, specifically ($\tau_h = \tau_l = 10$), yield the highest cooling rates at low values of ε. The extended interaction with both reservoirs allows more effective thermalization, resulting in a larger change in the internal energy of the working medium during the cooling stage. In contrast, symmetric configurations with the shortest thermalization times, ($\tau_h = \tau_l = 2.5$), exhibit the lowest cooling rates across the entire range of ε, indicating that insufficient thermal contact severely restricts energy exchange.

For asymmetric configurations with identical total cycle durations, the cooling rate is strongly influenced by the allocation of thermalization times. Configurations with longer interaction times with the hot reservoir produce higher

cooling rates than those dominated by extended contact with the cold reservoir. Physically, this indicates that the heating stage plays a dominant role in setting the energy scale of the cycle. A higher internal energy before the cooling stroke enhances the effective temperature difference during the subsequent isovolume cooling process, leading to increased heat extraction from the cold reservoir.

The reduction of the cooling rate at higher values of the coefficient of performance can be understood as a consequence of increased irreversibility and diminished temperature gradients under finite-time operation. As the system approaches higher efficiency, the effective temperature difference between the working medium and the reservoirs decreases, thereby suppressing the rate of heat transfer. This trade-off is an inherent feature of finite-time thermodynamics and cannot be eliminated.

In comparison with previous studies on finite-time quantum Otto refrigerators employing harmonic working media, the present results exhibit qualitative agreement, particularly regarding the trade-off between cooling rate and coefficient of performance (Abah et al., 2020; Abah and Lutz, 2016; Long and Liu, 2015). However, the sensitivity of the cooling rate to asymmetric thermalization times is significantly enhanced in the three-dimensional cubic trap considered here. This enhancement originates from the modified energy spectrum induced by the trap geometry, which amplifies the impact of partial thermalization on the thermodynamic behavior of the system.

4.4 Entropy production

Entropy production is a central measure of irreversibility in finite-time quantum refrigeration cycles. In a quantum Otto refrigerator, entropy changes arise solely during the isovolume heating and cooling processes, while the isentropic compression and expansion strokes do not contribute to entropy variation. As a result, the total entropy change during one thermodynamic cycle is determined by the balance between entropy generation during heating and entropy dissipation during cooling, both of which are strongly influenced by the respective thermal

contact durations. In general, the total entropy change over a complete cycle is given by eq. (3.6) For the working medium confined in a three-dimensional cubic trap, the entropy changes during the isovolume strokes are described by

$$\Delta S_{\text{heating}} = \frac{5}{2} k_B \left(\frac{m k_B}{2\pi\hbar^2}\right)^{3/2} \zeta\left(\frac{5}{2}\right) V_l \left[\left((T_2 - T_h)e^{-\alpha_h \tau_h} + T_h\right)^{3/2} - T_2^{3/2}\right], \tag{4.29}$$

$$\Delta S_{\text{cooling}} = \frac{5}{2} k_B \left(\frac{m k_B}{2\pi\hbar^2}\right)^{3/2} \zeta\left(\frac{5}{2}\right) V_h \left[\left((T_4 - T_l)e^{-\alpha_l \tau_l} + T_l\right)^{3/2} - T_4^{3/2}\right]. \tag{4.30}$$

Here, the entropy change during heating is positive because heat is absorbed from the hot reservoir, whereas the entropy change during cooling is negative due to heat release to the cold reservoir, consistent with the second law of thermodynamics (Zettira et al., 2024).

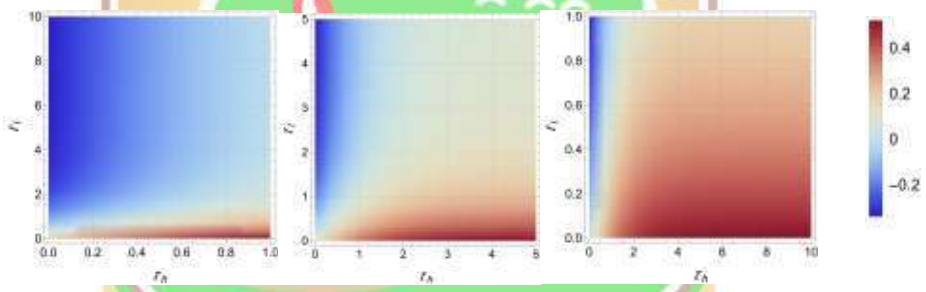

(a) (b) (c)

Figure 4. 5 The entropy change as a function of heating $\boldsymbol{\tau_h}$ (horizontal axis) and cooling $\boldsymbol{\tau_l}$ (vertical axis) stroke time, in the cases of: (a) $\boldsymbol{\tau_l = 10, \tau_h}$ = 1; (b) $\boldsymbol{\tau_l = \tau_h = 5}$; and (c) $\boldsymbol{\tau_l = 1, \tau_h = 10}$, with a compression ratio $\boldsymbol{\kappa = 2}$ and reservoirs temperatures $\boldsymbol{T_h = 45\ nK}$ and $\mathbf{T_l = 20\ nK}$.

Figure 4.5 presents the total entropy change as a function of the heating time τ_h and cooling time τ_l for three representative thermalization regimes: partial thermalization dominated by cooling ($\tau_l > \tau_h$), symmetric thermalization ($\tau_h = \tau_l$), and partial thermalization dominated by heating ($\tau_h > \tau_l$). These contour plots provide direct insight into how the allocation of thermal contact times governs entropy production in finite-time operation. In Fig. 4.5(a), corresponding to ($\tau_l > \tau_h$), the total entropy change becomes negative. This indicates that the magnitude

of entropy reduction during the cooling process exceeds the entropy increase generated during heating. Physically, the longer interaction with the cold reservoir allows the working medium to approach thermal equilibrium more closely, resulting in a more reversible heat release process. Consequently, entropy production is suppressed, making this regime thermodynamically favorable for refrigeration. This behavior is consistent with the cooling-rate analysis discussed previously, where extended cooling durations enhance heat extraction from the cold reservoir.

In contrast, Fig. 4.5(c) illustrates the regime ($\tau_h > \tau_l$), where the system remains in contact with the hot reservoir for a longer duration. In this case, the total entropy change is positive, indicating net entropy production. The prolonged heating stage promotes irreversible heat absorption, while the shortened cooling stage limits entropy dissipation to the cold reservoir. As a result, the entropy generated during heating cannot be sufficiently compensated during cooling, leading to increased irreversibility and degraded refrigeration performance.

The symmetric thermalization regime shown in Fig. 4.5(b) exhibits a balanced entropy distribution characterized by a diagonal transition from negative to positive entropy regions. The central area, where the total entropy change is close to zero, corresponds to near-reversible operation. This regime represents an optimal operating condition in which entropy production is minimized, allowing the refrigerator to maintain a favorable balance between cooling power and efficiency.

Overall, the entropy production analysis demonstrates that irreversibility in a finite-time quantum Otto refrigerator is highly sensitive to the relative durations of heating and cooling processes. While asymmetric thermalization can enhance certain performance metrics, such as cooling rate, it may also increase entropy production if the balance between heat absorption and heat release is not properly controlled. These results complement the cooling-rate and COP analyses presented earlier, emphasizing that optimal refrigeration performance is achieved through careful optimization of thermalization times rather than solely through reservoir temperatures or trap parameters.